

Chemical Vapor Deposition of Silica Micro- and Nanoribbons Using Step-Edge Localized Water

Michael P. Zach,[†] John T. Newberg, Luiza Sierra, John C. Hemminger, and Reginald M. Penner*

Department of Chemistry, University of California, Irvine, California 92697-2025

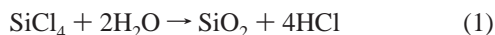
Received: February 21, 2003

Amorphous silica (SiO_2) ribbons were prepared by hydrolyzing SiCl_4 at highly oriented pyrolytic graphite (HOPG) surfaces on which water had condensed. Exposure to humid air ($>30\%$ relative humidity (RH)) at room temperature caused water to condense selectively at hydrophilic step edges on an otherwise hydrophobic graphite surface. Upon exposure of this surface to SiCl_4 vapor, a reaction with condensed water at step edges caused the formation of SiO_2 according to the reaction $\text{SiCl}_4 + 2\text{H}_2\text{O} \rightarrow \text{SiO}_2 + 4\text{HCl}$. The shape and size of the SiO_2 nanostructures varied with the RH: Below 20% RH, nanoparticles of SiO_2 , aligned at step edges, were observed. For RH of 35–50%, continuous nano- and microribbons of SiO_2 were obtained. For higher RH, micron-scale silica particles and ribbons were both observed. At a RH of 35%, silica ribbons as small as 80 nm (width) \times 20–40 nm (height) up to 500 μm in length could be prepared. Repetitive dosing of the HOPG surface in the humid environment with SiCl_4 produced nano- and microribbons with a height and width that increased in proportion to square root of the SiCl_4 dose.

I. Introduction

Micron-scale fibers composed of silicon dioxide and other dielectrics are technologically important as conduits for light.^{1,2} New methods for preparing dielectric nanofibers have recently emerged. Wang, Gole, and co-workers^{3–6} have described a technique for preparing “nanobelts” composed of a variety of metal oxides including SiO_2 , SnO_2 , ZnO , In_2O_3 , and others. These single crystalline structures are prepared by thermal evaporation and vapor transport of the metal oxide from powders at ≈ 1000 – 1400 °C. Wang et al.⁷ have also demonstrated that amorphous silica nanowires can be obtained by vapor–liquid–solid (VLS) synthesis at 1150 °C using gallium catalyst droplets. Wu and co-workers⁸ prepared amorphous SiO_2 nanowires by a carbothermal reduction reaction between silicon dioxide and activated carbons at 1350 °C. Leiber and co-workers^{9,10} have employed laser ablation to control the diameters of crystalline silicon nanowires prepared by VLS at 440 °C.

In this paper we demonstrate that graphite step edges can be used to template the formation of SiO_2 nanoribbons at room temperature using the strategy shown schematically in Figure 1. The basal plane surface of a highly oriented pyrolytic graphite (HOPG) crystal is traversed by a high density (10^3 – 10^4 cm^{-2}) of step edge defects that are approximately linear and up to a millimeter in length. These step edges can be used to template the growth by electrodeposition of metal¹¹ or conductive metal oxide (e.g., MoO_2)^{12,13} nanowires, but insulators such as SiO_2 cannot be electrodeposited. Upon equilibration of a graphite surface with humid air, water condenses preferentially at hydrophilic defects on the surface—especially step edges. SiO_2 nano- and microribbons were obtained by exposing this “wet” HOPG surface to the SiCl_4 vapor:



* Corresponding author. E-mail: rmpenner@uci.edu.

[†] Current address: Department of Earth and Planetary Sciences, University of California, Berkeley, California 94720-4767.

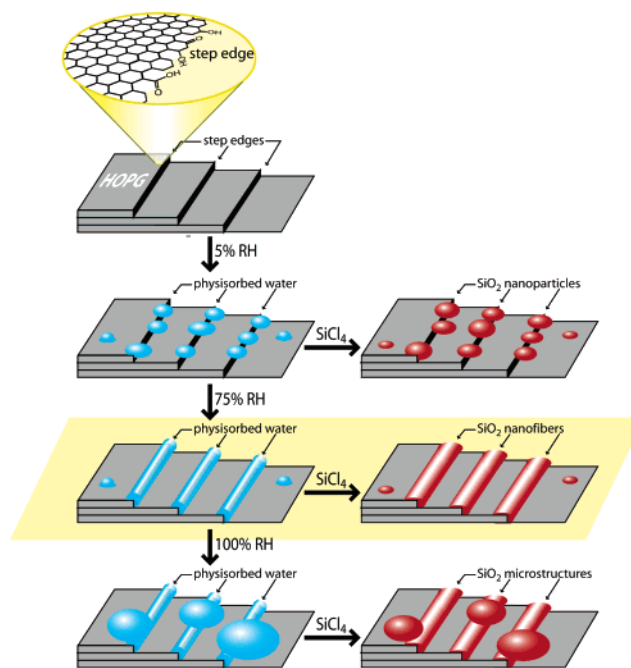


Figure 1. Method for forming SiO_2 micro- and nanoribbons on HOPG step edges at room temperature.

Previously, reaction 1 has been used to prepare silica films using atomic layer epitaxy (ALE) and atomic layer processing (ALP). In experiments by George et al.,^{14–16} silicon surfaces were exposed alternately to water and SiCl_4 under conditions where both reagents underwent surface-limited reactions. Ultrathin (<15 nm) silica layers of the desired thickness were thereby built up in 0.8–1.0 nm steps. Implementation of ALE involving reaction 1 has required either elevated temperatures (>600 K¹⁶) or the use of catalysts (NH_3 ,^{17,18} pyridine¹⁹). We demonstrate here that high-purity SiO_2 ribbons can be obtained using reaction 1 at room temperature without catalysts.

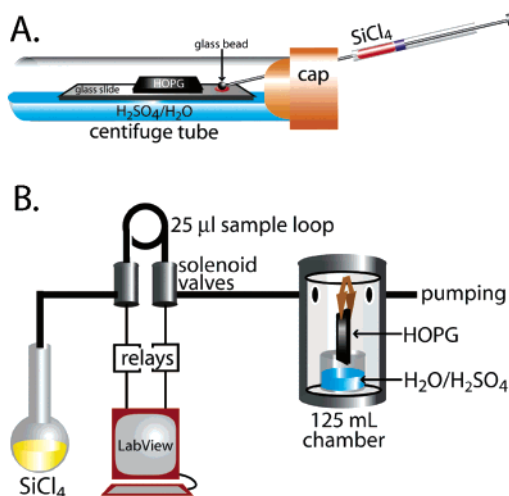


Figure 2. Experimental apparatuses used for creating nanoribbons in this work. (A) HOPG was suspended on a glass microscope slide within a plastic centrifuge tube containing a few milliliters of a sulfuric acid and water mixture. The relative humidity was adjusted using the concentration of acid (see Figure 3A). A syringe needle was inserted through the cap to deliver the SiCl_4 to a glass bead located 10 mm from the HOPG. The bead prevented liquid SiCl_4 from making direct contact with the HOPG. (B) A stainless steel reaction chamber facilitated precise dosing of the SiCl_4 onto the HOPG surface. The dosing was controlled by filling a 5 cm length of a stainless steel tube ($1/16$ in. diameter o.d., 0.4 mm i.d.) with argon and SiCl_4 vapor from a 200 mL glass vessel pressurized to 2 atm with argon and allowed to reach equilibrium with liquid SiCl_4 . Two Clippard solenoid valves were used to deliver 25 μL volumes of SiCl_4 vapor to the reaction chamber. These were either controlled manually or controlled via a computer interface and LabView. Additional ports to the chamber were used for a roughing pump, argon purge, thermocouple vacuum gauge, and a second dosing loop used for other reagents or independent water vapor dosing.

II. Experimental Methods

Silicon Dioxide Deposition. Two types of controlled humidity chambers were employed for the chemical vapor deposition of silicon dioxide step edge coatings in this work. The first consisted of a capped 50 mL polypropylene disposable centrifuge tube (Figure 2A). The humidity in these tubes was fixed by equilibrating the interior of the tube with several milliliters of a sulfuric acid/water mixture. The HOPG crystal was placed on the glass microscope slide that spanned the width of the centrifuge tube. After an equilibration time of at least 15 min, ~ 0.05 mL of SiCl_4 (99.998%, Aldrich) was delivered onto a 4 mm glass bead affixed to the glass slide ~ 10 mm away from the graphite crystal on the glass slide. The evaporation and reaction of SiCl_4 with adsorbed water occurred within seconds but the graphite was maintained in the tube for 5 min to ensure the reaction was complete. HOPG samples were then removed into ambient laboratory air and analyzed by AFM, SEM, TEM, SAED, EDAX, and XPS (see below).

A stainless steel chamber with a volume of 150 mL was specially built to carry out experiments in which HOPG surfaces were exposed to pulses of SiCl_4 vapor while in a controlled humidity environment. The dosing system attached to this chamber consisted of a glass flask containing a few milliliters of SiCl_4 pressurized to 1 atm with argon. Two solenoid valves separated the flask from the main chamber with a stainless steel loop (volume = 25 μL) connecting the two valves. With the loop evacuated to the pressure of the main chamber (< 6 mTorr), the first valve to the flask would be held open and the dosing loop was allowed to fill with argon saturated with SiCl_4 vapor. With the first valve closed the second valve was then opened and allowed to dump its contents to the chamber. This procedure was repeated to deliver additional doses of SiCl_4 . HOPG crystals were freshly cleaved and suspended by a copper alligator clip over a 50:50 mixture of H_2SO_4 and water, resulting in a RH = 37%.

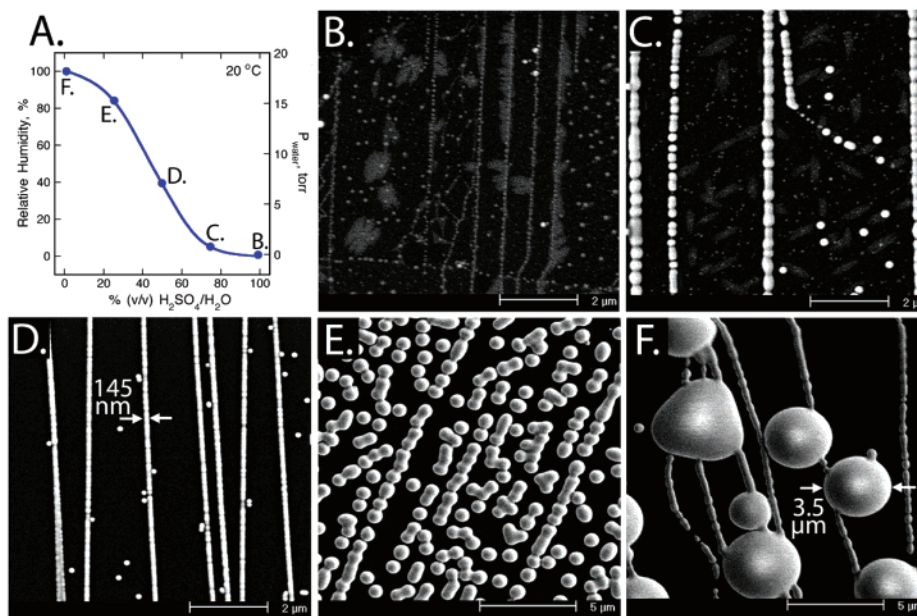


Figure 3. SEM images showing the effect of the humidity on the selectivity of SiO_2 deposition and showing the morphology of the resulting deposit. These samples were prepared using the apparatus shown in Figure 2A. (A) The sulfuric acid–water solution in the centrifuge tube produced a constant humidity in accordance with the relationship plotted here. The SEM images shown in (B)–(F) were acquired at the humidity values indicated in this diagram. (B) Virtually no deposition was observed for HOPG surfaces equilibrated near 0% RH (over pure H_2SO_4). (C) At $\sim 6\%$ RH, deposition of SiO_2 was confined to step edges, but discontinuous structures were obtained. (D) At $\sim 37\%$ RH, SiO_2 was again confined to step edges, and many of these “nanoribbons” were continuous for hundreds of microns. (E) At $\sim 84\%$ RH, SiO_2 deposited both at terraces and on step edges. These deposits had a beaded appearance. (F) At 100% RH (over pure water), micron scale hemispheres of SiO_2 were observed on top of decorated step edges.

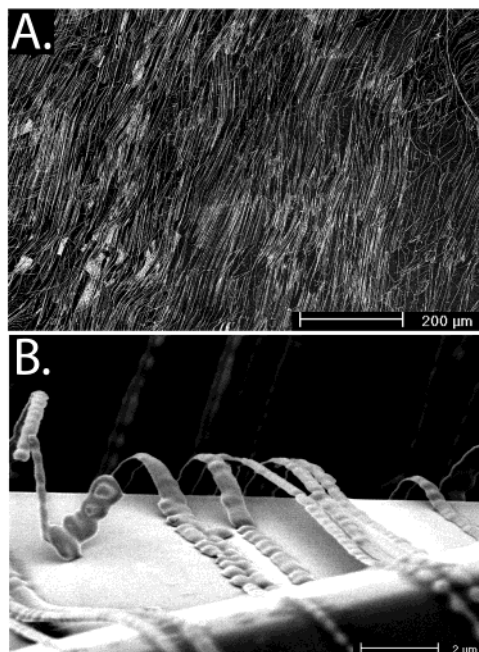


Figure 4. Two SEM images of silica nanoribbons prepared using 37% RH and the apparatus of Figure 2A. (A) This low magnification image shows the organization of nanoribbons on the HOPG surface. This organization is a reflection of the organization of step edges on the HOPG surface. Many of the silica nanoribbons on this surface exceeded 0.5 mm in length. (B) Silica ribbons are flexible and can be removed from the substrate by flexing the HOPG. This perspective image shows a closeup of an area that has been folded. The mechanical properties of these ribbons, coupled with their weak adhesion to the HOPG surface, allows one to separate the ribbons from the HOPG surface, giving free-standing ribbons.

X-ray Photoelectron Spectroscopy. X-ray photoelectron spectroscopy (XPS) was carried out using an ESCALAB MKII photoelectron spectrometer (VG Scientific). The ESCALAB MKII is a multitechnique surface analysis instrument based on an ultrahigh vacuum (UHV) system consisting of three separately pumped, interconnected chambers (sample preparation, fast sample entry, and spectroscopy). The fast entry chamber allowed rapid sample transfer from air to UHV pressures (base pressures during XPS analysis were in the low-to-mid 10^{-10} Torr range). The XPS experiments were performed in the spectroscopy chamber using a standard Mg anode X-ray source (and the Mg $K\alpha$ X-rays at 1253.6 eV) and a 150 mm hemispherical electron energy analyzer. The spectra presented here were acquired using an analyzer pass energy of 20 eV. Under these conditions the spectrometer energy resolution was ~ 0.8 eV. Samples were prepared by supporting the graphite surface, upon which the nanowires were prepared, on a copper sample holder using conductive colloidal silver paste (Ted Pella). Binding energies were referenced to the C(1s) peak at 284.5 eV.

Microscopy. Scanning electron microscopy (SEM) was carried out on uncoated samples using a Philips FEG-30XL microscope equipped with EDAX elemental analysis capabilities. TEM was performed on a Phillips CM-20. Noncontact AFM was accomplished using a Park Scientific Instruments Autoprobe CP with a noncontact head, a 10 μm scanner, and noncontact Ultralevers (A and B tips with resonant frequencies of 70–90 kHz).

Additional Dielectric Materials Deposited. All other depositions were done using the centrifuge tubes with the equilibration of the HOPG done over the 50:50 $\text{H}_2\text{SO}_4/\text{H}_2\text{O}$ mixture while the same air-sensitive syringe techniques were observed. Titanium dioxide was deposited from the TiCl_4 precursor

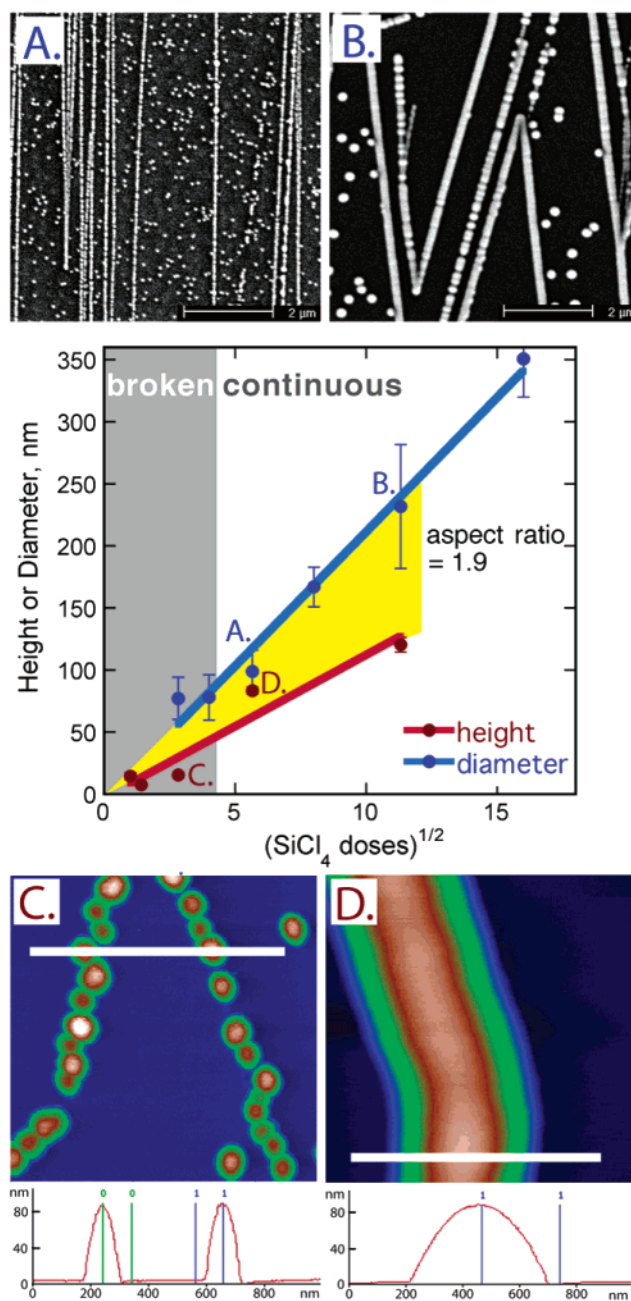


Figure 5. Plots of average width (or diameter) and average height as a function of the number of SiCl_4 doses for silica ribbons prepared using the apparatus shown in Figure 2B. In these experiments, the HOPG surface was equilibrated with argon at 37% RH. SEM images were used to extract the widths; AFM images were analyzed to determine the ribbon heights. The error bars shown in this Figure represent $\pm 1\sigma$ for the mean value for each data point. (A), (B) SEM images of the surface after 32 and 128 doses. (C), (D) AFM images and topography traces of the surface after 8 and 128 doses.

(99.9%, Aldrich). Germanium oxide was deposited from the GeCl_4 precursor (99.99%, Aldrich).

III. Results and Discussion

The strategy outlined in Figure 1 was first implemented using closed, polypropylene centrifuge tubes (volume = 50 mL, Figure 2A). A few milliliters of a sulfuric acid/water mixture at the bottom of these tubes fixed the relative humidity (RH) according to the relationship plotted in Figure 3A. A graphite crystal was placed on a glass slide suspended over this sulfuric acid solution.

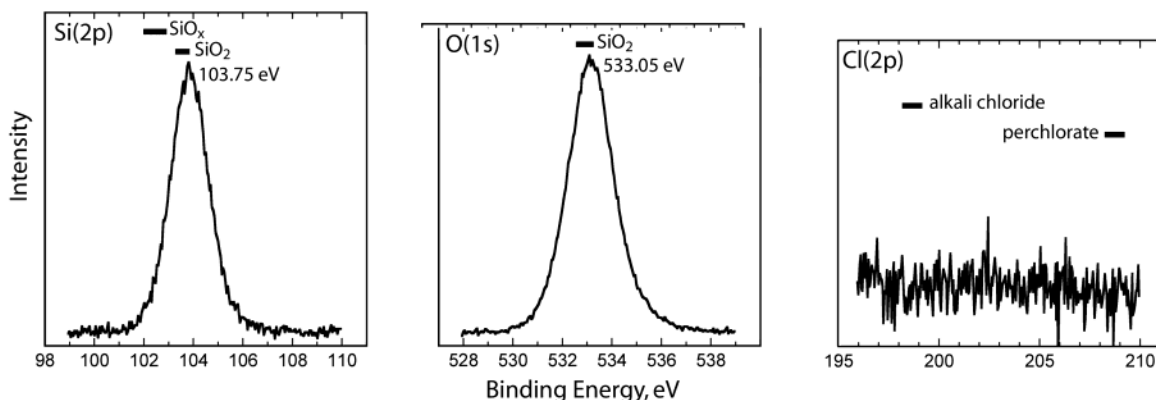


Figure 6. X-ray photoelectron spectra of an HOPG surface prepared in the apparatus of Figure 2A using RH = 37%. Si(2p) and O(1s) binding energies are both consistent with SiO₂. The Cl(2p) region showed no detectable chloride. The binding energy ranges indicated in this figure were obtained from ref 20.

After an equilibration period of at least 15 min, a $\approx 50 \mu\text{L}$ droplet of SiCl₄ was syringed onto a 4 mm glass bead affixed to the glass slide, located 10 mm away from the graphite crystal. This glass bead prevented liquid SiCl₄ from contacting the HOPG. SiCl₄ vapor was then permitted to diffuse and react with adsorbed water on the graphite surface. This process was complete in an instant, but 5 min was allowed to ensure complete reaction of all precursor.

Scanning electron microscopy (SEM) images of graphite surfaces prepared using this procedure are shown in Figure 3. In dry air (equilibrated with 100% H₂SO₄), almost no SiO₂ was observed on the graphite surface, as shown in Figure 2B. For RH from 10 to 20%, exposure of the graphite to SiCl₄ caused the formation of hemispherical nanometer and micron-scale particles composed of SiO₂, as seen in Figure 3C. These particles formed preferentially at defect sites of the HOPG surface (especially step edges) because these defects are hydrophilic whereas the surrounding defect-free basal plane is hydrophobic. As the RH was increased to between 30 and 45%, the quantity of condensed water increased and the condensate at step edges evolved into continuous hemicylindrical ribbons or “wires”. A RH value of 37% was close to optimum in terms of favoring this morphology for the silica deposit. Exposure of this surface to SiCl₄ resulted in the formation of SiO₂ ribbons at steps as seen in Figure 3D. If the graphite surface was equilibrated with RH >60%, droplets of water formed at both defects, and also on defect-free regions of the basal plane. The corresponding morphology of the SiO₂ obtained at these high humidities is shown in Figure 3E,F.

In Figure 4 two SEM images show the silica nano- and microribbons formed using this procedure at RH $\approx 37\%$. The parallel nature of step edges on cleaved graphite results in the formation of large arrays of parallel silica ribbons, as seen clearly in the low magnification SEM image of Figure 4A. It is also apparent from this image that many thousands of silica ribbons with lengths of 200–500 μm were produced in a typical experiment. The length of the individual ribbons is a reflection of the fact that step edges can traverse the entire diameter of the columnar grains within the HOPG. For the ZYB grade HOPG utilized for these experiments, many of these grains had diameters in excess of 500 μm . Thus, in a typical CVD experiment, many thousands of silica ribbons with lengths of 200–500 μm were produced. Typical SiO₂ ribbons can be seen in the cross-section of the SEM image shown in Figure 4B. Bending the graphite surface caused these SiO₂ fibers to release from the surface. These SiO₂ fibers were ribbon-shaped with an aspect ratio ($A = \text{width/height}$) of 2–5.

A higher degree of control over the silica growth process was obtained using a stainless steel reaction chamber in conjunction with a system for delivering pulses of SiCl₄ vapor. The apparatus we employed, shown schematically in Figure 2B, allowed SiCl₄ vapor to be delivered in identical 25 μL pulses into a 150 mL stainless steel reaction chamber that was evacuated to <6 mTorr and maintained at an RH close to 37% using 1:1 H₂SO₄:H₂O. The pulse duration and the equilibration time between pulses were both 1 s. We measured the mean width of silica ribbons using SEM (e.g., Figure 5A,B) and the mean height using atomic force microscopy (AFM, Figure 5C,D) as a function of the number of SiCl₄ pulses, N . Both dimensions increased smoothly with N , and in direct proportion to $N^{1/2}$. Assuming the reaction probability at nascent silica ribbons remains constant over the duration of the experiment, the increase in both the width and height is predicted to be linear with the square root of the number of pulses applied, as shown by eq 2:

$$r(N) = \sqrt{\frac{2\alpha N P_{\text{SiCl}_4} V_{\text{SiCl}_4} V_m}{A\pi R T l}} \quad (2)$$

In this equation, N is the number of SiCl₄ pulses, α is the fraction of the injected SiCl₄ that reacts with nascent silica ribbons, P_{SiCl_4} is the vapor pressure of SiCl₄ at 23 °C (~ 0.255 atm), V_{SiCl_4} is volume of SiCl₄ injected with each pulse, V_m is the molar volume of the SiO₂, A is the aspect ratio of the semi-elliptical SiO₂ wires, and l is the total length of active step edges. Figure 5 also shows the threshold at which ensembles of SiO₂ particles arrayed along step edges coalesced into continuous ribbons. We found that the smallest continuous silica ribbons obtainable using this approach were approximately 75 nm in diameter and 45 nm in height. These dimensions were achieved using four SiCl₄ pulses under the conditions of our experiment. A smaller number of pulses produced hemispherical silica particles along step edges, as shown in the AFM image of Figure 5C.

Transmission electron microscopy (TEM) and selected area electron diffraction (SAED) of these silica nanowires revealed them to be amorphous. Energy-dispersive X-ray elemental analysis (EDAX) showed the presence of silicon and oxygen. Contaminating elements were not detected.

A more quantitative assessment of the quality of the silica produced using this approach was possible using X-ray photoelectron spectroscopy. Shown in Figure 6 are the Si(2p), O(2s), and Cl(2p) regions of the spectra for a freshly prepared sample. The Si(2p) chemical shift can be used to distinguish SiO₂ from

SiO_x ($x < 2$). The observed shift of 103.75 is at the high-energy limit of the region normally associated with SiO₂. Residual surface chlorine was not observed, indicating that HCl volatilized from the surface, and the reaction proceeded to completion.

In principle, the method described here is extendable to a variety of hydrolyzable precursors such as GeCl₄ (for the synthesis of GeO₂), (CH₃)₃Al (for Al₂O₃), and TiCl₄ (for TiO₂). In preliminary experiments, we have demonstrated that nano- and microribbons are obtained for all three of these precursors, but additional optimization of the deposition conditions will be required before the quality of these other dielectrics is at the level seen for SiO₂ here.

Acknowledgment. This work was funded by the National Science Foundation (CHE-0111557). M.P.Z. acknowledges support from the American Chemical Society, Division of Analytical Chemistry Fellowship sponsored by Merck and Company. J.C.H. acknowledges funding support from the Department of Energy through contract DE-FG03-96ER45576. Finally, we thank Dr. Art Moore of Advanced Ceramics Inc. for donations of graphite.

References and Notes

- (1) Balzer, F.; Rubahn, H. G. *Surf. Sci.* **2002**, *507*, 588.
- (2) Balzer, F.; Rubahn, H. G. *Appl. Phys. Lett.* **2001**, *79*, 3860.

- (3) Gole, J. L.; Stout, J. D.; Rauch, W. L.; Wang, Z. L. *Appl. Phys. Lett.* **2000**, *76*, 2346.
- (4) Wang, Z. L.; Dai, Z. R.; Gao, R. P.; Bai, Z. G.; Gole, J. L. *Appl. Phys. Lett.* **2000**, *77*, 3349.
- (5) Pan, Z. W.; Dai, Z. R.; Wang, Z. L. *Science* **2001**, *291*, 1947.
- (6) Pan, Z. W.; Dai, Z. R.; Wang, Z. L. *Appl. Phys. Lett.* **2002**, *80*, 309.
- (7) Pan, Z. W.; Dai, Z. R.; Ma, C.; Wang, Z. L. *J. Am. Chem. Soc.* **2002**, *124*, 1817.
- (8) Wu, X. C.; Song, W. H.; Wang, K. Y.; Hu, T.; Zhao, B.; Sun, Y. P.; Du, J. J. *Chem. Phys. Lett.* **2001**, *336*, 53.
- (9) Morales, A. M.; Lieber, C. M. *Science* **1998**, *279*, 208.
- (10) Cui, Y.; Lauhon, L. J.; Gudiksen, M. S.; Wang, J. F.; Lieber, C. M. *Appl. Phys. Lett.* **2001**, *78*, 2214.
- (11) Favier, F.; Walter, E. C.; Zach, M. P.; Benter, T.; Penner, R. M. *Science* **2001**, *293*, 2227.
- (12) Zach, M. P.; Ng, K. H.; Penner, R. M. *Science* **2000**, *290*, 2120.
- (13) Zach, M. P.; Inazu, K.; Ng, K. H.; Hemminger, J. C.; Penner, R. M. *Chem. Mater.* **2002**, *14*, 3206.
- (14) George, S. M.; Ott, A. W.; Klaus, J. W. *J. Phys. Chem.* **1996**, *100*, 13121.
- (15) Klaus, J. W.; Sneh, O.; Ott, A. W.; George, S. M. *Surf. Rev. Lett.* **1999**, *6*, 435.
- (16) Klaus, J. W.; Ott, A. W.; Johnson, J. M.; George, S. M. *Appl. Phys. Lett.* **1997**, *70*, 1092.
- (17) Klaus, J. W.; George, S. M. *Surf. Sci.* **2000**, *447*, 81.
- (18) Klaus, J. W.; George, S. M. *J. Electrochem. Soc.* **2000**, *147*, 2658.
- (19) Klaus, J. W.; Sneh, O.; George, S. M. *Science* **1997**, *278*, 1934.
- (20) Moulder, J. F.; Stickle, W. F.; Sobol, P. E.; Bomben, K. D. *Handbook of X-ray Photoelectron Spectroscopy*; Perkin-Elmer Corp.: Eden Prairie, MN, 1992.